J. Fluid Mech. (1994), *vol.* 281, *pp.* 219–245

Experiments in a boundary layer subjected to free stream turbulence. Part 2. The role of TS-waves in the transition process

By A. V. BOIKO[2], K. J. A. WESTIN[1], B. G. B. KLINGMANN[1]†, V. V. KOZLOV[2] AND P. H. ALFREDSSON[1]

[1]Department of Mechanics/Fluid Physics, Royal Institute of Technology, S-10044 Stockholm, Sweden

[2]Department of Theoretical and Applied Mechanics, Russian Academy of Sciences, Siberian Branch, 630090 Novosibirsk, Russia

(Received 17 November 1993 and in revised form 8 July 1994)

The natural occurrence of Tollmien–Schlichting (TS) waves has so far only been observed in boundary layers subjected to moderate levels of free stream turbulence ($Tu < 1\%$), owing to the difficulty in detecting small-amplitude waves in highly perturbed boundary layers. By introducing controlled oscillations with a vibrating ribbon, it is possible to study small-amplitude waves using phase-selective filtering techniques. In the present work, the effect of TS-waves on the transition is studied at $Tu = 1.5\%$. It is demonstrated that TS-waves can exist and develop in a similar way as in an undisturbed boundary layer. It is also found that TS-waves with quite small amplitudes are involved in nonlinear interactions which lead to a regeneration of TS-waves in the whole unstable frequency band. This results in a significant increase in the number of turbulent spots, which promote the onset of turbulence.

1. Introduction

'Natural' Tollmien–Schlichting (TS)-waves induced by free stream turbulence (FST) were first identified by Schubauer & Skramstad (1948), who disturbed the free stream by placing a rope grid in the settling chamber of their wind tunnel. Compared to the undisturbed free stream case, this gave a visible increase in the wave activity, which hastened the development of pre-transitional structures and turbulent spots. The boundary layer gradually becomes turbulent as both the number of turbulent spots and their size increase downstream.

The role of TS-waves in transition induced by FST has become a subject of discussion only recently. Some authors (e.g. Morkovin 1984; Suder, O'Brien & Reshotko 1988) claim that at FST levels above 1%, TS-waves play no role in transition, and suggest that some other, as yet unknown, mechanism is at work, termed by them 'by-pass' mechanism. However, the usefulness of this concept is limited, since the authors do not specify the characteristic features of the postulated mechanism. More insight may instead be gained by comparing experimental observations in the boundary layer under FST to phenomena known from basic studies on transition, in

† Present address: Volvo Aerospace Corp., Space Propulsion Division, S-461 81 Trollhättan, Sweden.

order to identify the active mechanism(s), and relate them to the external conditions. A brief overview of known transition scenarios and receptivity conditions is therefore given in the following subsections.

The purpose of the present experiments is to investigate the behaviour of TS-waves at turbulence levels $Tu > 1\%$. At such levels of FST, TS-waves are difficult to identify because of the large level of fluctuations inside the boundary layer, which increase both with Reynolds number and with Tu. The present experiments extend a series of studies by Grek, Kozlov & Ramazanov (1987, 1990*a,b*, 1991*b*; in the following referred to as GKR), performed under similar conditions in the T-324 wind tunnel of the Institute of Theoretical and Applied Mechanics of the Russian Academy of Science in Novosibirsk. GKR studied a boundary layer subjected to grid-generated FST with $Tu = 1.35\%$. TS-waves were excited by means of a vibrating ribbon placed inside the boundary layer, and their downstream development was followed using analogue filtering of the hot-wire signal around the generation frequency. The waves were seen to amplify linearly, but at a lower amplification rate than in the absence of FST. The ribbon-generated TS-wave was also found to induce energy in a broad band of frequencies for which TS-waves are unstable, and the number of turbulent spots increased with increasing ribbon amplitude. TS-waves and turbulent spots were seen to co-exist in the boundary layer, without visibly affecting each other. Similar observations were also made in an accelerating boundary layer. The observations by GKR are confirmed and extended in the present study, using improved methods of wave detection.

Section 2 gives a brief description of the experimental set-up (further details can be found in part 1 of the present report (Westin *et al.* 1994) and in Klingmann *et al.* 1993). The signal processing procedure used to separate TS-waves from other boundary layer perturbations is described in § 3. In § 4 it is shown that TS-waves can be excited by a vibrating ribbon inside the highly perturbed boundary layer in the presence of FST, and that waves which remain coherent during their downstream travel amplify in an amplitude-independent (i.e. linear) way. However, amplitude-dependent (nonlinear) effects can be observed even at quite small wave amplitudes. These observations are presented in § 5, and provide a basis for the discussion of the role of TS-waves in FST-induced transition in § 6.

1.1. *Some notes on receptivity*

FST excites at least two types of motions in the boundary layer: TS-waves in the form of randomly occurring wave packets; and low-frequency fluctuations, which start to develop from the leading edge of the plate, and account for the major part of the r.m.s. velocity fluctuations (u_{rms}) inside the boundary layer (these are sometimes referred to as 'Klebanoff-modes'). The relative importance of these two motions depends on the efficiency of the forcing and on conditions favouring their development in the boundary layer. Their role in transition may also depend on possible mutual interactions.

In a flow visualization by Gulyaev *et al.* (1989), it can be observed how vortices from the free stream impinge onto the boundary layer and there develop into packets of streaky flow structures which are carried downstream by the flow. The low-frequency fluctuations observed in hot-wire measurements are thought to be caused by the random occurrence of such streak packets. As shown in part 1, the intensity of the low-frequency motion grows downstream at a rate proportional to the Reynolds number (R), and attains levels of $5 - 13\%$ of the free stream velocity (U_0) before transition occurs. In general, the growth rate increases with Tu. However, the

intensity of the low-frequency r.m.s. at the onset of transition differs widely between different experiments, even between experiments carried out at similar levels of Tu. This means that the transition point can not be directly inferred from the intensity of the streaks, and their precise role in the transition process is not clear.

'Natural' TS-waves have been observed at low levels of FST by (among others) Arnal & Juillen (1978), Suder *et al.* (1988), Kendall (1985, 1990, 1991) and Kosorygin & Polyakov (1990). In all cases, TS-wave packets similar to those found by Schubauer & Skramstad (1948) were observed. Kosorygin & Polyakov studied the downstream development of these wave packets, and found that they amplify at the same rate as two-dimensional TS-waves in the undisturbed boundary layer. Kendall, on the other hand found that their growth rate depends on Tu, and may exceed amplification rates in the undisturbed boundary layer. In the experiments by Kosorygin & Polyakov, the growth was simply defined from the downstream increase of energy in the spectral components corresponding to unstable TS-wave frequencies, whereas Kendall used a more sophisticated method to separate TS-waves from the background fluctuations. Wave packets were detected by using differential pressure sensors, where each side of the membrane was connected to the wall by a pair of orifices. By choosing the orifice spacing to about half a TS-wavelength, the sensitivity to TS-waves was high compared with fluctuations with other wavelengths. It should be noted that the growth rates measured by Kosorygin & Polyakov and by Kendall represent the overall increase in the number and size of TS-wave packets, rather than the amplitude growth within a packet. Whether this growth is due to a continuous downstream forcing from the free stream, or to processes developing inside the boundary layer is difficult to distinguish. This can only be achieved by introducing controlled TS-waves, as in the experiments by GKR. They found that TS-waves amplify at a lower rate than in the undisturbed boundary layer.

To what extent TS-waves play a role in a given practical situation may depend on a number of circumstances, such as the efficiency with which they are triggered from the free stream, the relevant Reynolds number range, pressure gradients and leading edge conditions. The effect of the leading edge flow on the stability of TS-waves in an undisturbed environment was demonstrated by Klingmann *et al.* (1993). At low Tu, Kendall (1991) found that TS-waves are more efficiently excited when the leading edge is blunt, or when the model is placed at a positive angle of attack, i.e. when an adverse pressure gradient favours their amplification. On the other hand, an unfavourable pressure distribution near the leading edge may lead to transition before the growth of TS-waves becomes significant, e.g. in the experiments by Suder *et al.* (1988), the early transition may be due to a suction peak near the leading edge. This was also observed in the present experiment, when the leading edge flow was intentionally deteriorated (see part 1).

It is well known that pressure gradients along the chord strongly affect the amplification of TS-waves. The low-frequency fluctuations induced by FST, however, seem to be insensitive to pressure gradients (see Kendall 1991; V. E. Kozlov *et al.* 1990). It is therefore noteworthy that Blair (1992), in an experiment at $Tu = 2\%$, observed a significant delay of the onset of transition when the flow acceleration was increased, so that the boundary layer became stable with respect to TS-waves. If the observations made by Kendall and V. E. Kozlov *et al.* are generally valid, the effect observed by Blair seems to be the result of an efficient suppression of TS-waves by the negative pressure gradient. This gives an indication of the important role TS-waves may also play in the transition of a flat-plate boundary layer at high levels of FST.

1.2. *Mechanisms of transition*

Whereas the evolution of large-scale structures in the boundary layer is rather slow and undramatic even at r.m.s. levels around 10% of U_0, TS-waves may develop nonlinear interactions at amplitudes below 1%, leading to a resonant three-dimensional amplification and rapid transition to turbulence.

The most thoroughly studied transition scenario starts with the linear amplification of TS-waves in an otherwise undisturbed boundary layer. The waves grow up to a point where nonlinear mechanisms lead to a resonant amplification of three-dimensional wave pairs. These intensify and form characteristic Λ-shaped structures consisting of inclined high-shear layers, which subsequently break down to turbulence. Depending on the forcing conditions, the nonlinear interactions may be either of fundamental (K) or subharmonic (N) type. The former was first investigated by Klebanoff, Tidstrom & Sargent (1962), whereas the latter was discovered by the Novosibirsk group (cf. Kachanov & Levchenko 1984). Mixed or 'detuned' types may also occur. A detailed discussion on the relative importance of different kinds of TS-wave interactions is given e.g. by Kachanov (1987), Zelman & Maslennikova (1993) and Kachanov (1994). In general, forcing at a large amplitude ($\geqslant 1\%$), e.g. by sound, favours the K-type, whereas subharmonic resonances occur at smaller wave amplitudes and may be expected under most 'natural' conditions.

The presence of broad-band low-frequency noise favours subharmonic TS-wave interactions. This was shown in an experiment by Gaster (1990), who studied the effect of combining a forced TS-wave with synthetic broad-band noise. As a result, energy is generated within a broad band of frequencies below the frequency of the TS-wave (these spectra are quite similar to those measured by GKR when TS-waves were forced in the presence of FST). The induced energy amplifies at a rate which is proportional to the square of the TS-wave amplitude. At high levels of forcing of the TS-wave, the dominant parts of the spectrum are centred around the subharmonic and its reflection in the fundamental (forced) frequency. The observed broad-band behaviour may well be the result of subharmonic interactions with different degrees of detuning.

The effect of FST on the laminar boundary layer may be seen as a continuous forcing by impulsive, localized disturbances. Useful information for understanding the transition process may therefore be obtained from experiments on the development of such disturbances. With the aim of modelling 'natural' TS-wave transition, Gaster & Grant (1975) studied the development of a TS-wave packet from a transient disturbance in the form of an air pulse from a small hole in the wall. Later studies (cf. Konzelmann 1990; Fasel 1990; Cohen, Breuer & Haritonidis 1991) revealed the detailed structure of the wave packet inside the boundary layer. It consists of a core of narrow, intense streaks surrounded by warped wave fronts. The subharmonic route to transition was observed by both Konzelmann and by Cohen *et al.* Since the streak packet propagates faster than the waves, it may travel ahead of the wave packet and develop separately (see Breuer & Haritonidis 1990). It decays if the initial disturbance is weak, and only if the initial forcing exceeds a certain threshold can the streak packet develop into a turbulent spot without involving the amplification of TS-waves (see Grek, Kozlov & Ramazanov 1985, 1990*b*; Klingmann 1992; Henningson, Lundbladh & Johansson 1993). The arrow-head shape of the streak packet is similar to Λ-structures resulting from TS-wave interactions, and transition is preceded by the formation of high-shear layers like those observed at the late stage of TS-wave transition. This is seen most strikingly in the visualization by Grek *et al.* (1990*b*). These phenomena have also been observed in transition induced

by FST. Visualizations by Kendall (1985) in the cross-stream plane show how the streaks lift up into pairs of inclined shear layers, and begin to roll up into streamwise vortices. In a recent numerical simulation of a boundary layer subjected to FST (Rai & Moin 1991), there are clear examples of the development of high-shear layers and associated phenomena, which can be identified with events known to occur in N- and K-transition as well as in transition caused directly by transient disturbances. This emphasizes the need to examine the development prior to the emergence of Λ-structures and high-shear layers, in order to assess the critical conditions causing them.

Possible interactions between TS-waves and large-scale structures resulting from an impulsive three-dimensional source have been studied by Grek *et al.* (1991*a*) and Grek & Kozlov (1992). Transient disturbances were introduced in different ways, both from the wall and from the free stream, and triggered the development of large-scale structures, which the authors termed 'puffs' (a puff is essentially identical to the above mentioned streak packets studied by Breuer & Haritonidis 1990, and Klingmann 1992). TS-waves were excited using a vibrating ribbon, and the interaction between the two was found to result in a nonlinear wave packet, which developed into a turbulent spot. This process was also observed under circumstances where both the puff and the TS-waves would decay if they were generated separately. Such interactions may also be expected in boundary layers subjected to FST.

2. Experimental set-up and measurement technique

The experiments were performed in the MTL (Minimum Turbulence Level) wind tunnel at the Royal Institute of Technology, Stockholm, Sweden. A general sketch of the set-up is shown in figure 1. The boundary layer over a flat plate with zero pressure gradient was studied. Near-isotropic FST with a level of $Tu = 1.5\%$ was generated by a square mesh grid, installed in the test section 1.5 m upstream of the plate (Tu is here defined as the r.m.s.-value of the streamwise velocity measured outside the boundary layer near the leading edge, normalized with U_0). The streamwise velocity was measured with a constant-temperature hot-wire anemometer, using single wires made of 5 μm platinum with a sensing length of 1 mm. Further details on the set-up, and a description of the free stream characteristics can be found in part 1. Most of the measurements were performed in set-up I, which is identical to that used by Klingmann *et al.* (1993), except for the presence of the grid – in fact some of the measurements were carried out simultaneously.

A major concern in the present experiment was the flow near the leading edge, since the pressure distribution there may affect the receptivity of the boundary layer with respect to TS-waves, and may also favour the generation of turbulent spots. As demonstrated by Klingmann *et al.* (1993), the leading edge affects the initial development of the boundary layer (and consequently the TS-wave development at low R, i.e. large F). A flow which smoothly accelerates from the stagnation line was achieved here by a special design of the leading edge in combination with a trailing edge flap for adjustment of the stagnation line (see figure 2*a* in part 1). This arrangement is similar to that in the experiments by GKR, who used a leading edge with the shape of an asymmetric dual ellipse with a high aspect ratio. In some of their early experiments, turbulent spots occurred due to leading edge effects. To a minor extent, this may also have been the case in the present experiments. The pressure distribution with and without the grid is shown in figure 2(*b*) in part 1. The effect is quite small, and is limited to a region < 20 mm from the leading edge. Further

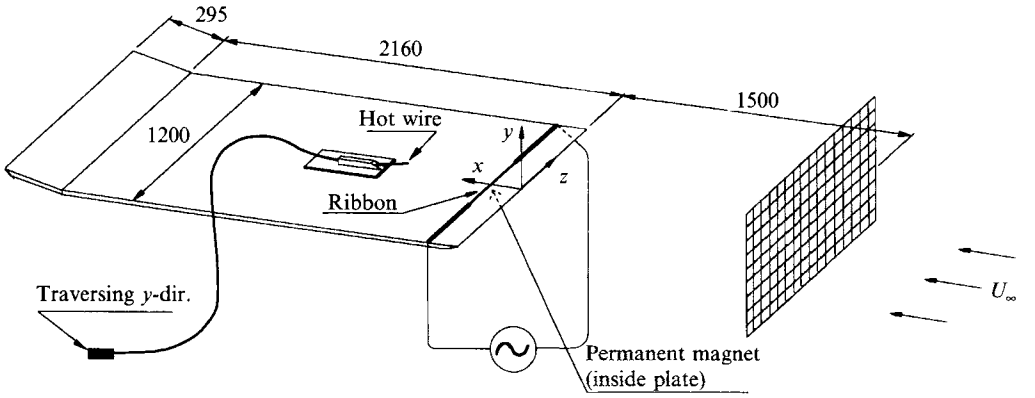

FIGURE 1. Experimental set-up. Dimensions in mm.

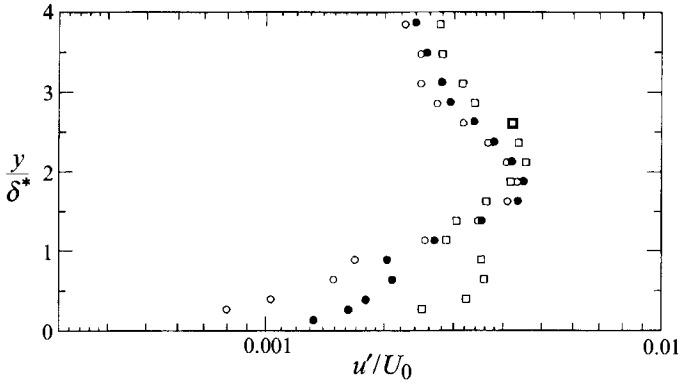

FIGURE 2. Profiles of u'_F at different ribbon amplitudes: ○, G_1; ●, G_2; □, G_3. $F = 100$, $x = 500$ mm ($R = 890$).

downstream, the difference in the pressure coefficient (C_p) with and without the grid is within 0.5% and does not show any consistent trend. Since in the present set-up the insertion of the grid introduces no significant changes of the pressure distribution, it was not deemed necessary to readjust the trailing edge flap after inserting the grid.

Periodic waves were excited by a vibrating ribbon positioned 120 mm downstream of the leading edge. The ribbon was placed in the field of a permanent magnet mounted in a hollow on the reverse side of the plate, and was brought into vibration by feeding it with an electric current of the desired amplitude and frequency. This was controlled by a function generator via an audio amplifier, an 8 Ω resistor and a 220/33 V transformer. The hot wire signal and the signal feeding the vibrating ribbon were sampled simultaneously by a MacADIOS-adio A/D converter connected to a Macintosh SE/30. Care was taken to minimize possible channel interference in the A/D converter. For this purpose, the signal from the frequency generator was attenuated through a variable potentiometer before it was passed to the A/D converter. Special tests were performed to ensure that the contributions from channel leakage were at least $10^2 - 10^3$ times smaller than the measured wave amplitudes.

The streamwise, wall-normal and spanwise directions are denoted by x, y and z respectively. Measurements were undertaken in the region from $x = 150$ to 1000 mm from the leading edge ($x = 0$), at free stream speeds between 4 and 8 m s^{-1}. The

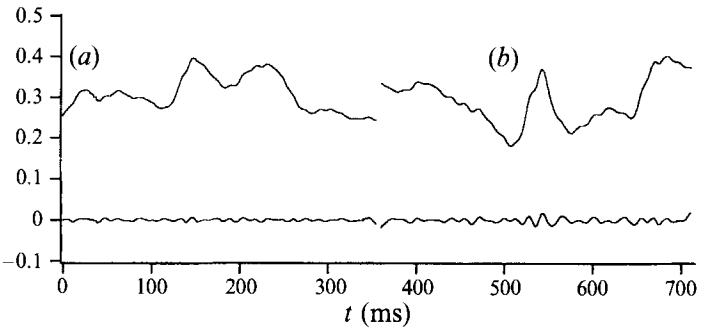

FIGURE 3. Typical hot-wire signals (full signal and high-pass filtered above 30 Hz) obtained near the inner maximum of u'_F. (*a*) $x = 700$ mm ($R = 1050$), (*b*) 1000 mm ($R = 1260$). Ribbon working at $F = 100$, amplitude G_1.

Reynolds number is defined as $R = 1.72R_x^{1/2}$, where $R_x = U_0 x/\nu$, and the frequency parameter $F = 10^6 \times \omega\nu/U_0^2$, where ω is the angular frequency, and ν the kinematic viscosity.

3. Signal processing

When the boundary layer fluctuations (u_{rms}) are small, TS-waves can readily be detected due to the fact that their maximum amplitude occurs close to the wall, where the overall boundary layer perturbations give only minor contributions to typical TS-wave frequencies. In general, u_{rms} increases with Tu and R, and at some point the waves can no longer be observed by merely looking at oscilloscope traces or power spectra. By generating TS-waves in a controlled manner, their frequency and phase are well defined, which greatly facilitates the study of their mode shape and downstream evolution. In the experiments of GKR, controlled TS-waves were examined at $Tu = 1.35\%$. The waves were extracted from the background perturbations with an analogue spectrum analyser by narrow-band-pass filtering close to the generator frequency, and contributions from turbulent spots were sorted out 'by eye'. In the present study, the experimental set-up and approach are similar, but a refined technique was used to study the waves.

Figure 2 shows profiles of narrow-band filtered r.m.s.-fluctuations (u'_F), when the ribbon is operated at 70 Hz with different amplitudes ($G, G_1 < G_2 < G_3$). The measurement was made at $x = 500$ mm ($R = 890$). The forcing frequency ($F = 100$) is within the range of unstable frequencies for TS-waves in a Blasius boundary layer ($F = 70 - 150$ at $R = 890$). The outer maximum in the profiles in figure 2 is due to background disturbances, which for $F = 100$ have their maximum far out in the boundary layer (see also figure 12 in part 1). The near-wall maximum, which for the highest amplitude (G_3) amounts to 0.35% of U_0, contains contributions both from the triggered waves and from other boundary layer fluctuations with the same frequency. Typical hot-wire signals obtained at the near-wall maximum, are shown in figure 3, where the lowest ribbon amplitude (G_1) was used. The waves, which are riding on large-scale background structures, appear more clearly when the signal is high-pass filtered (see lower traces in figure 3). In order to separate the waves from random-phase contributions with the same frequency, a phase-selective filtering technique was used which will be described below.

A large number (N, typically 100) of sampling records, each containing 512 samples,

were collected using sampling frequencies between 360 and 720 Hz. Each record was then phase aligned with respect to the generator source. By ensemble averaging the phase-aligned records, only that part of the signal which is phase-coherent with the frequency generator will contribute to the ensemble average, whereas contributions with random phase are attenuated when N is large. A straightforward method of phase alignment is to trigger the start of the sampling sequence from the signal controlling the ribbon. For technical reasons, however, a different method was used in the present study. In each record the phase of the spectral component corresponding to the generator frequency was compared with the phase of the generator, whereupon the spectra were phase shifted with the calculated phase difference. The procedure can be described as follows.

If the ribbon is operated by a generator signal with an angular frequency ω_g,

$$\hat{G}e^{-i\omega_g t},$$

the ω_g-component of the signal acquired at a given x- and y-position can be assumed to consist of a wave component

$$\hat{A}e^{i(\alpha x-\omega_g(t-t_0))},$$

and random-phase contributions

$$\hat{R}e^{i(\phi_R-\omega_g t)}$$

at the same frequency. (Here t_0 represents the time it takes for the wave to travel downstream to the the point of measurement, and α is the wavenumber.) All Fourier components of the measured signal were multiplied with the complex conjugate of the generator signal, and after ensemble averaging, the following quantity is extracted from the ω_g-component:

$$\hat{B}e^{-i\omega_g t} = \frac{1}{N\hat{G}}\sum_{n=1}^{N}[\hat{A}e^{i(\alpha x-\omega_g(t-t_0))} + \hat{R}e^{i(\phi_{R,n}-\omega_g t)}]\,[\hat{G}e^{-i\omega_g t}]^* = \hat{A}e^{i(\alpha x-\omega_g t_0)} + \frac{1}{N}\sum_{n=1}^{N}\hat{R}e^{i\phi_{R,n}}.$$

In this way, the ensemble average contains only the phase-coherent part of the ω_g-component, whereas for large enough N, fluctuations with other frequencies or phases are cancelled out in the averaging process. In order to avoid end effects, the generator frequency was carefully matched to the discrete sampling frequency. The final values of amplitude and phase were obtained after an additional 4 Hz wide Gaussian filtering.

This method provides the possibility of extracting the amplitude and phase distributions in the outer parts of the boundary layer also, where fluctuations with random phase give the main contributions to the energy at ω_g. Figure 4 demonstrates how the method works. Power spectra and phase-averaged spectra are shown at two different y-positions, corresponding to the near-wall TS-wave maximum (*a* and *c*) and the boundary layer edge (*b* and *d*). The waves were forced with G_1 at 70 Hz ($F = 100$), and the signals were collected at $x = 500$ mm ($R = 890$). Near the wall, the wave is clearly visible in the spectrum (figure 4*a*), but its true amplitude is obscured by contributions from other boundary layer perturbations. In the corresponding phase-aligned spectrum (figure 4*c*), the contributions to the 70 Hz component are reduced from 0.21 to 0.12, i.e. almost by a factor of 2. At the boundary layer edge, the generated wave is completely invisible in the spectrum (figure 4*b*), due to the high level of background disturbances near the frequency of interest, and phase alignment is necessary here to detect the wave. A large number of records is required in order to reduce the

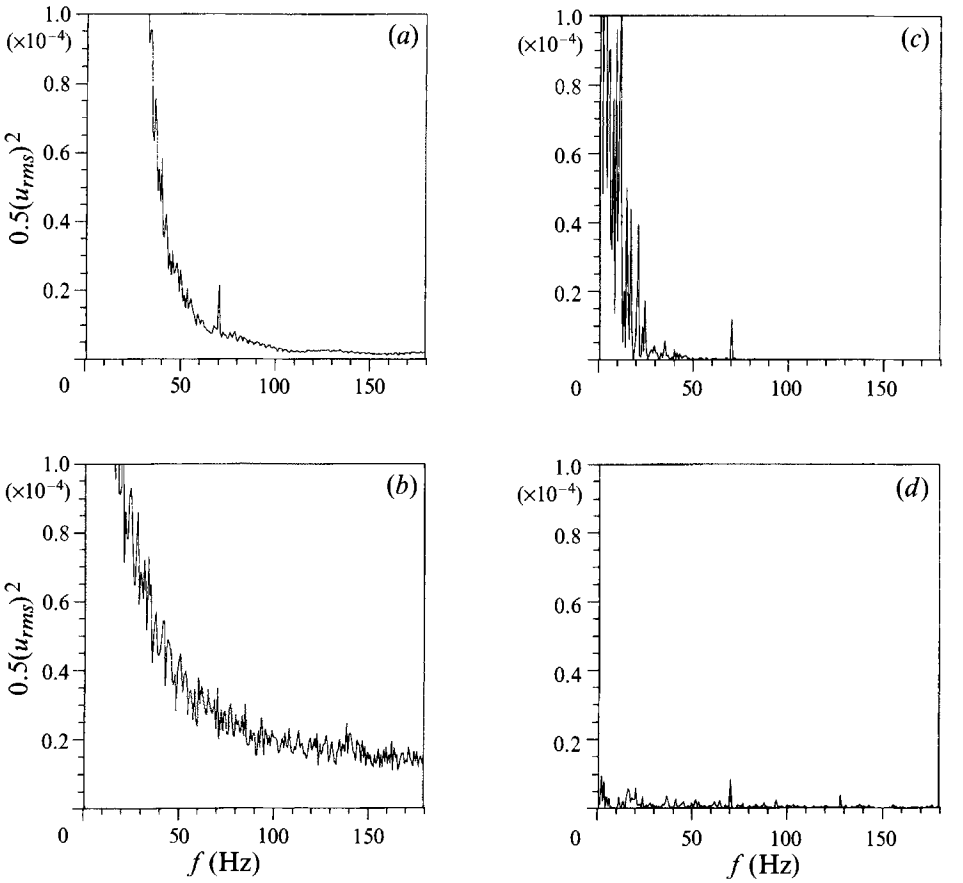

FIGURE 4. Extraction of ribbon-induced waves from background fluctuations by means of phase-aligned averaging. (*a,b*) Power spectra inside the boundary layer and close to the boundary layer edge respectively, (*c,d*) spectra after phase alignment. x = 500 mm (R = 890), F = 100. Amplitude G_1.

unphased contributions, and insufficient averaging easily results in an over-estimation of the true amplitude of the wave. Because of the downstream growth of the total u_{rms} level, the extraction becomes more difficult as the wave is followed downstream. However, it was possible to extract and follow TS-waves with amplitudes as small as 0.02% of U_0.

Records which were affected by the passage of a turbulent spot were sorted out using a simple threshold criterion on $\partial u/\partial t$. If the velocity increased by more than $0.35U_0$ between two consecutive samples, the sampled record was discarded, and a new record was collected. This procedure eliminated the influence of intermittent turbulent spots on the measured spectra, and also allowed estimation and comparison of the number of spots observed at different x-positions and forcing amplitudes.

4. Linear development of TS-waves

A TS-wave is here defined as a small-amplitude wave, characterized by its amplitude and phase distribution through the boundary layer, as well as the propagation speed and amplification rate, which can be predicted by linear stability theory at any given

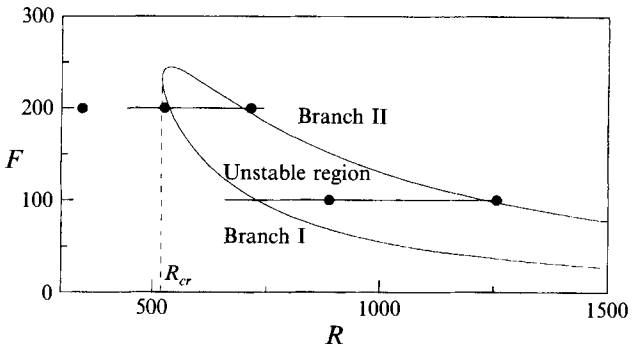

FIGURE 5. Neutral stability diagram for TS-waves in the Blasius boundary layer (linear parallel theory). Symbols show working points for profile measurements, lines the region where amplification was measured.

frequency and Reynolds number. The neutral stability curve obtained from linear parallel theory is shown in figure 5. It encloses the region where two-dimensional TS-waves are amplified, and the left and right parts of the curve are denoted branch I and branch II respectively. In the absence of the grid, neutral points in good agreement with this curve were obtained in the present set-up, and also at frequencies near $F = 200$ (see Klingmann *et al.* 1993). The working points at which the present study was conducted are also shown in figure 5.

Since the downstream evolution of TS-waves does not follow the self-similar evolution of the boundary layer, the measured amplification rates will in general depend on the y-position at which the amplitude is measured. The near-wall amplitude maximum with respect to y at a given x-position is in the following denoted by A in the absence of the grid, and by B in its presence. At each x-position, A and B were determined separately by traversing over a few points in y near the wall. Their values are given in % of U_0. The integrated amplification (N) at a given station x is defined as

$$N = \ln \frac{A}{A_0} \text{ without the grid,}$$

or

$$N = \ln \frac{B}{B_0} \text{ with the grid,}$$

where the subscript $_0$ refers to the amplitude measured at branch I. The TS-wave amplitude measured in the absence of the grid at branch II of the neutral stability curve will be denoted by A_{II}.

Linear stability calculations were carried out using either the Orr–Sommerfeld equation, or the 'parabolized stability equations' (PSE, cf. Bertolotti, Herbert & Spalart 1992). The spatial formulation of the Orr–Sommerfeld equation gives an eigenvalue problem for the determination of the complex wavenumber α. The growth or decay of the wave is then obtained as the imaginary part of the wavenumber, α_i, and N is calculated as

$$\int_{x_0}^{x} -\alpha_i \mathrm{d}x.$$

The wave is damped if α_i is positive and amplified if α_i is negative. The eigenvalue problem was solved using an iterative shooting method, where the eigenfunctions were computed by integrating the Orr–Sommerfeld equation using a fourth-order

Runge–Kutta scheme with orthogonalization. The boundary conditions at infinity were obtained from the asymptotic solution of the equation as $U \to U_0$ (cf. Jordinson 1970). The PSE contain several extra terms which describe the growth of the boundary layer and the modification of the mode shape of the wave with x. The equations are derived by keeping terms up to $O(R^{-2})$ in the linearized Navier–Stokes equations, where the streamwise derivative $(\partial/\partial x)$ is assumed to be of $O(R^{-1})$. The PSE-code is based on a spectral method using an expansion in Chebyshev polynomials in the y-direction, and a first-order backward Euler scheme in the streamwise marching procedure.

4.1. *Linear stability predictions for the mean flow perturbed by FST*

It is well known from linear stability theory that even small changes in the mean velocity profile can significantly affect the stability of TS-waves. It is therefore plausible to expect that the modification of the mean velocity profile in the presence of FST would affect the TS-wave growth. Although it must be kept in mind that the flow is three-dimensional and non-stationary, an indication on the tendency of this effect (stabilizing or destabilizing) may be obtained by applying two-dimensional linear stability theory on the measured mean velocity profiles.

The deviations of the mean velocity from a Blasius profile (ΔU), measured at $x = 800$ mm ($R = 1125$), are shown in figure 6(*a*) as a function of the boundary layer coordinate y/δ^* (δ^* is the measured displacement thickness). In part 1, it was found that the shape of this profile is self-similar, whereas its magnitude increases downstream, giving a continuous decrease in the shape factor (H) (at $x = 800$ mm, $H = 2.43$). A curve fit to the measured values of U was constructed by fitting a high-order polynomial to $\Delta U(y/\delta^*)$, and was then added to the Blasius profile. This is shown in figure 6(*a*) (solid line) for $x = 800$ mm ($R = 1125$), and U'' (the second y-derivative of U) is shown in figure 6(*b*). It is negative at all y-positions, but its magnitude is smaller and the maximum is closer to the wall in comparison to the Blasius profile. For comparison, ΔU and U'' for a Falkner–Skan profile with $H = 2.43$ are also shown in figures 6(*a*) and 6(*b*) (dashed lines). Although qualitatively similar to the measured data, the details in the Falkner–Skan profile are different, in particular the wall shear stress is larger than for the measured data.

The predicted TS-wave amplification rate is highly sensitive to minor changes in U'', and near the wall the profiles cannot be measured with an accuracy high enough to correctly estimate this quantity. A straightforward polynomial fit produces unreasonable variations in the near-wall curvature, unless some constraint is applied on U''. In the curve fit shown in figure 6(*a,b*), U'' was forced to 0 at the wall. Using this as an input to linear, parallel stability calculations gave a damped wave with $\alpha_i\delta^* = +0.0057$ for $F = 100$. A milder restraint on U'' is obtained by adding a number of interpolated values to the measured data near the wall. This gives values of $\alpha_i\delta^*$ varying between $+0.0012$ and $+0.0041$, i.e. in all cases a damped wave is predicted. For reference, the Blasius profile gives an amplifying TS-wave with $\alpha_i\delta^* = -0.0053$, whereas the Falkner–Skan profile is strongly damped with $\alpha_i\delta^* = +0.0120$. Since ΔU is self-similar, the same procedure could easily be repeated at other x-positions by simply adjusting the amplitude of the fitted curve to the measured shape factor. At all positions, the stability calculation predicted damped waves for $F = 100$.

In summary, the influence of FST may be expected to stabilize the mean velocity profile with respect to two-dimensional TS-waves.

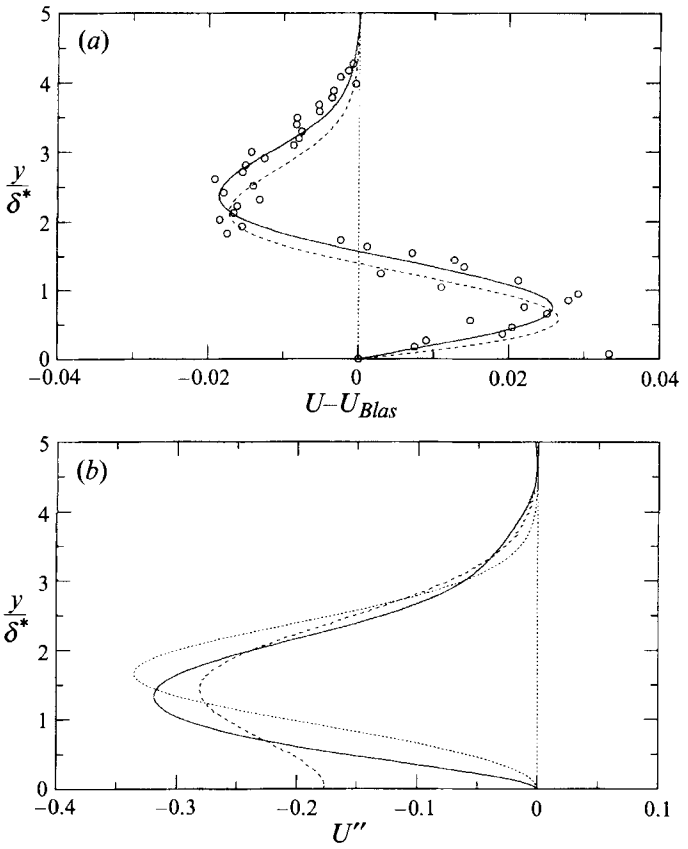

FIGURE 6. (*a*) Mean velocity deviation from the Blasius profile, (*b*) second derivative of the mean velocity profile. ○, Experiment; —, polynomial curve fit to the experimental data; – – –, Falkner-Skan flow; · · · , Blasius flow. $x = 800$ mm ($R = 1125$), $H = 2.43$.

4.2. *Measured TS-wave characteristics in the presence of FST*

Figure 7 shows amplitude and phase distributions of ribbon-induced waves, extracted with the filtering technique described in § 3. The location of the working points with respect to the neutral stability curve for TS-waves is shown in figure 5. Figure 7(*a*) compares profiles measured with and without the grid at $F = 200$. The free stream velocity was 4 ms^{-1}, and the value of u_{rms}/U_0 in the middle of the boundary layer was 5% at the most downstream position. The data were obtained by phase-averaging 100 records at each y-position. The three x-positions shown are close to the ribbon ($x = 150$ mm, $R = 345$), close to branch I of the neutral stability curve ($x = 350$ mm, $R = 525$) and close to branch II ($x = 650$ mm, $R = 715$). Worth mentioning is the short downstream distance required to set up a TS-wave, which can be seen at $x = 150$ mm, i.e. a distance less than one TS-wavelength downstream of the vibrating ribbon ($\lambda_{TS} = 48$ mm). At all three positions, the wave extracted in the presence of the grid shows the same characteristic features as a TS-wave in an undisturbed boundary layer. The near-wall maximum, followed by a 180° phase shift and a second outer maximum can clearly be seen. One can also observe the downstream changes in the wave shape, which are due to the fact that the shape of the TS-wave is not self-similar with the growing boundary layer. The inner maximum as well as the phase shift are slowly displaced towards the wall, both with and without the grid. At

the more downstream positions, the contributions from random fluctuations increase, giving a considerable scatter in the data points if the number of averaged records is not large enough. This is particularly obvious close to the amplitude minimum and the corresponding phase shift.

Figure 7(*b*) shows amplitude and phase profiles for $F = 100$. The free stream velocity was 8 ms^{-1}, and the two downstream positions shown are $x = 500$ and 1000 mm ($R = 890$ and 1260). Each profile is constructed from the phase-average of 50 records at each y-position. Also shown are the corresponding TS-wave profiles calculated for the Blasius boundary layer. For the latter, $R = 890$ is at the beginning of the unstable region, and $R = 1260$ is just downstream of branch II. With the grid inserted, this position can still be considered as upstream of the onset of transition, and turbulent spots appeared only occasionally. When introducing controlled TS-waves, the number of spots increased significantly, an observation which will be further discussed in the following section. The maximum in u_{rms}/U_0 with respect to y was 7.5% at $R = 890$ and 11% at $R = 1260$. Nevertheless, it was possible to extract a phase-coherent wave with an amplitude and phase distribution resembling a TS-wave, although the agreement is not as good as in figure 7(*a*). Both the inner and the outer maxima as well as the amplitude minimum are clearly visible in the profile, but their locations and magnitudes differ from that of an undisturbed TS-wave. The large amplitude of the outer maximum is at least partly due to insufficient averaging. The phase shift is not as distinct as it should be for a TS-wave, but varies more smoothly. Despite these differences, it is clear that the generated wave survives at far downstream distances and maintains its TS-like character in a highly disturbed (but still laminar) boundary layer.

Figure 8 shows the evolution of the phase versus x for $F = 100$ and 200. The phase speed, evaluated from the slope of the straight lines through the data points, is indistinguishable for the cases with and without the grid – it is $0.405U_0$ for $F = 200$ and $0.37U_0$ for $F = 100$. The amplitude evolution of the extracted wave is shown in figure 9 for $F = 100$, 150 and 200, together with the corresponding amplification curves for TS-waves measured in the absence of the grid. Also shown are the corresponding curves obtained from linear two-dimensional parallel/non-parallel theory. The latter is in good agreement with the amplification curves measured in the absence of the grid. The waves extracted in the presence of the grid are also amplified, but the measured amplification rates are smaller, and damping sets in further upstream than in the undisturbed case.

The observed decrease in the amplification rate as compared to the case without FST could be attributed to a number of possible effects. The first question is whether the amplification rate can simply be caused by small pressure gradient effects which may be introduced when the grid is inserted. An amplification curve similar to figure 9(*c*) would be obtained in a mildly accelerating flow, e.g. a Falkner–Skan flow with constant $H = 2.56$, which in the present case would correspond to a decrease in the pressure coefficient C_p by 2–8% per metre in the region $x = 250$ to 1000 mm. However, the pressure distribution with the grid shows no such tendency, and the difference in C_p measured with and without the grid was within 0.5% in the present set-up (see also figure 2*c* in part 1). Pressure gradient effects may therefore be ruled out. Another question is to what extent the increased wall shear stress in the boundary layer with FST may act as stabilizing on TS-waves. The two-dimensional stability calculations in § 4.1 indicate that the mean velocity profile with the grid is completely stable with respect to TS-waves at $F = 100$, while figure 9(*c*) shows that they are

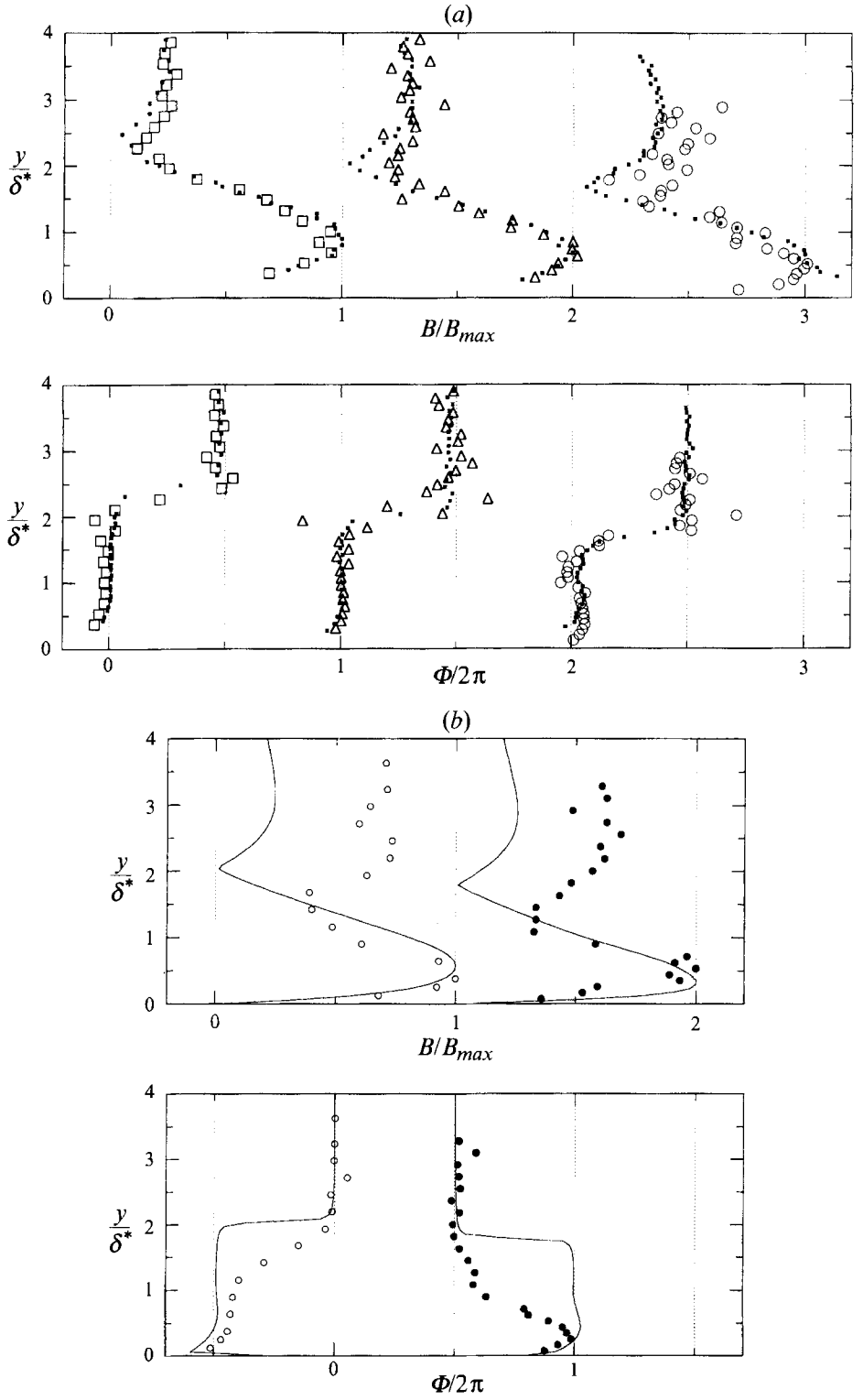

FIGURE 7. Amplitude and phase profiles of ribbon-excited TS waves in the presence of FST (*a*) $F = 200$, $U_0 = 4$ ms^{-1}; □, $x = 150$ mm ($R = 345$); △, $x = 350$ mm ($R = 525$); ○, $x = 650$ mm ($R = 715$); dots show profiles measured without the grid. (*b*) $F = 100$, $U_0 = 8$ ms^{-1}; ○, $x = 500$ mm ($R = 890$); •, $x = 1000$ mm ($R = 1260$); solid lines show profiles obtained from linear, parallel stability theory.

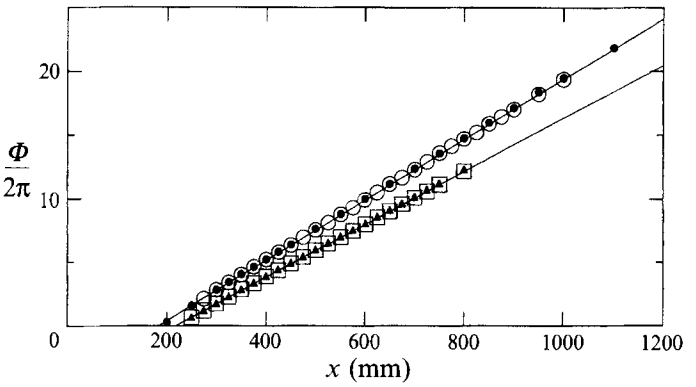

FIGURE 8. Phase evolutions for $F = 200$: ○, with and ●, without the grid; $F = 100$: □, with and ▲, without the grid.

	G_1	G_2	G_3
Output voltage fed to the ribbon	3.85 V	9.5 V	18.5 V
Maximum wave amplitude for $F = 100$			
without the grid (A_{II})	0.4%	1.0%	$\geqslant 1\%$
with the grid (B)	0.15%	0.35%	0.65%

TABLE 1. Relation between ribbon forcing and measured wave amplitudes

amplified. Hence, it is clear that a simple quasi-steady two-dimensional approach cannot give satisfactory predictions of the stability of TS-waves in this flow.

The amplification rate of the extracted wave was independent of the ribbon amplitude. This is shown in figure 9(*d*) for $F = 100$. The ribbon amplitudes were chosen from measurements without the turbulence-generating grid, whereupon the grid was installed and the same output signal was fed to the ribbon. The relation between the forcing of the ribbon and the maximum measured wave amplitudes is given in table 1. In the absence of the grid, the waves attain their highest amplitude at $R = 1220$, where, for the three ribbon amplitudes G_1, G_2 and G_3, the values of A_{II} are 0.4%, 1% and $\geqslant 1\%$ respectively. With the grid inserted, the maximum value of B occurred further upstream, and was 0.15%, 0.35% and 0.65% respectively, i.e. about three times smaller than in the absence of the grid. The amplification curves in figure 9(*d*) are normalized at $R = 550$, and the curves for all three amplitudes are seen to coincide (to within experimental scatter), showing that the development of the extracted wave is independent of amplitude. Hence, the waves seem to amplify within the linear regime.

So far we have seen that it is possible to generate and detect waves with TS-like characteristics in a highly disturbed boundary layer. Such waves may exist in boundary layers subjected to high levels of FST, even if they are not directly visible in oscilloscope traces or power spectra. The measured amplitude and phase distributions exhibit typical TS-wave features. Phase coherent waves with such characteristics can be detected all the way to the beginning of transition. They travel downstream at the same speed as undisturbed TS-waves, but seem to amplify less. These results confirm the previous findings by GKR that TS-like waves may exist and develop despite the high level of disturbances in the boundary layer.

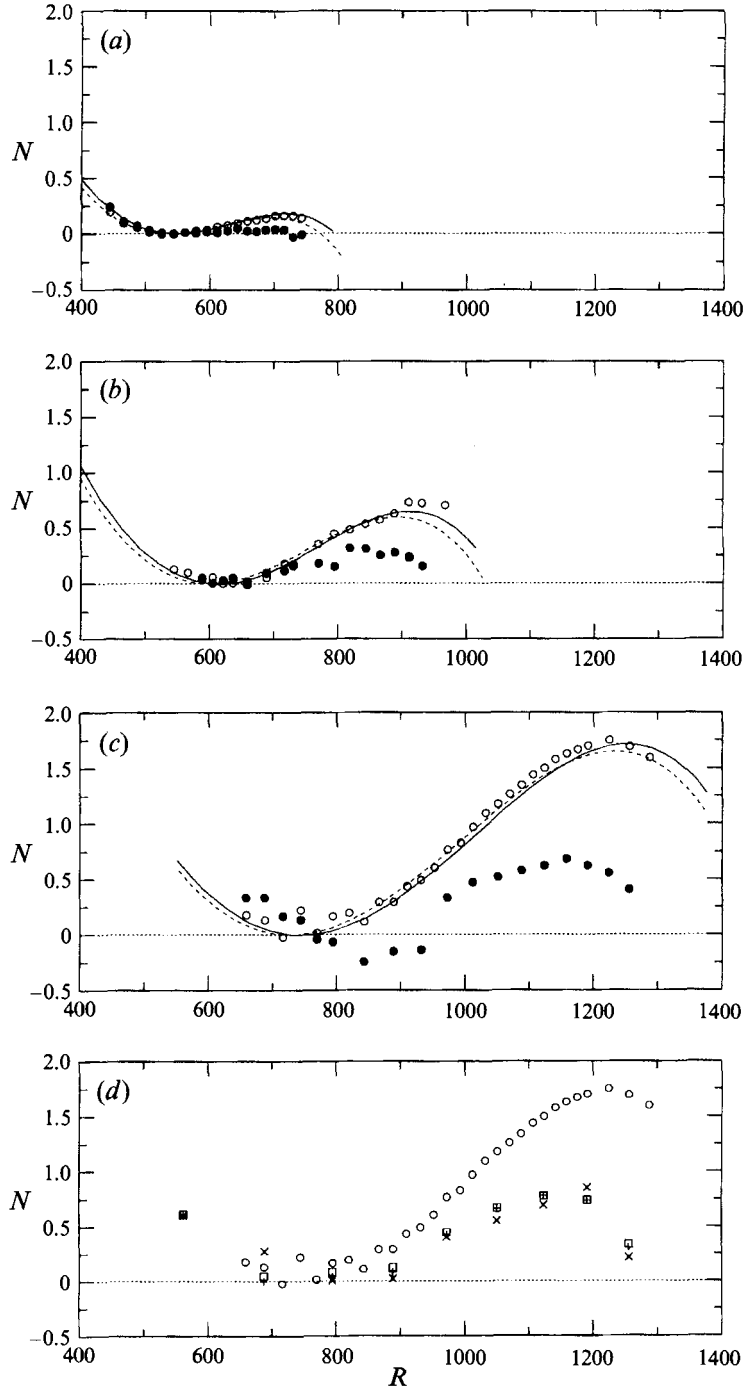

FIGURE 9. Amplitude evolutions with and without the grid. (*a*) $F = 200$, (*b*) $F = 150$ and (*c*) $F = 100$. •, With the grid; ○, without the grid; —, PSE calculation; – – –, linear, parallel theory. (*d*) $F = 100$, different ribbon amplitudes. With the grid: ×, G_1; +, G_2; □, G_3. ○, without the grid.

5. The effect of TS-waves on transition

During the measurements reported above, it was observed that the introduced TS-waves affect the transition process, most easily recognized from the increased number of transitional structures and turbulent spots detected during the data acquisition. The intermittency increased with the ribbon amplitude, and at the largest amplitude, the number of spots increased dramatically. This was also observed in the previous studies by GKR. The dependence of this phenomenon on the ribbon amplitude indicates that the formation of turbulent spots is due to some nonlinear process which involves the TS-waves.

5.1. *Response to varying forcing amplitudes*

By looking at oscilloscope traces at a far downstream position, some qualitative observations can be made, which may give some hints about the nature of these interactions. The observations described in the following were made just downstream of branch II in the stability diagram, at $F = 100$ and $R = 1260$.

In the absence of the grid, the three forcing amplitudes G_1, G_2 and G_3 give TS-waves with the maximum amplitudes $A_{II} = 0.4\%$, 1% and $\geqslant 1\%$ respectively. For the lowest ribbon amplitude, the wave amplifies according to linear theory down to branch II, and then damps, while for the amplitudes G_2 and G_3, nonlinear phenomena associated with the N- and K-routes to transition were observed. The onset of nonlinearity can be clearly seen in the spectra and can also be observed directly in the oscilloscope traces. The first sign of subharmonic (N-type) interactions is a variation of the maximum amplitude in time during two successive wave periods, accompanied by an irregular, low-frequency modulation of the wave train. Fundamental interactions (K-type) are seen as a distortion of the sinusoidal wave shape, while the wave train remains regular. Figure 10 compares the spectra at a streamwise position close to branch II, obtained with two different levels of forcing (without the grid). In figure 10(*a*), the forcing was between G_1 and G_2, and the spectrum contains only the forced wave frequency. Figure 10(*b*) shows the appearance of peaks both at the sub- and superharmonic frequencies when the forcing level is increased to G_2 ($A_{II} = 1\%$). The subharmonic is detuned, as can be seen from the double peak centred on the subharmonic frequency. There is also an increase of energy at very low frequencies, which reflects a slow modulation of the wave train. Another indication of nonlinear wave interactions is that the amplification rate becomes smaller compared to the linear case. This was observed for the forcing amplitude G_2, for which the interactions were subharmonic in the absence of the grid (cf. Klingmann *et al.* 1993). For the largest forcing amplitude (G_3), the predominant interactions are of fundamental (K) type. Regular 'peaks' and 'valleys' develop along the span, indicating the formation of aligned Λ-structures. In this case, the determination of A_{II} is ambiguous, since the amplitude varies with the spanwise position.

With the grid, the measured wave amplitudes were considerably lower than without it (the highest measured amplitude with G_3 at branch II was 0.65% of U_0). Figure 11(*a–c*) shows selected oscilloscope traces with the grid, obtained at a y-position near the inner amplitude maximum of the TS-wave. Each plot contains three independent time series, and the lower traces show the same signal high-pass filtered above 30 Hz. For the lowest ribbon amplitude shown in figure 11(*a*) (G_1) the generated waves appear to be superimposed on the large-scale structures which have a timescale of the order of 100 ms (10 Hz), sometimes interrupted by transitional structures or incipient turbulent spots with much larger amplitudes. It is interesting to note that almost identical structures, with a timescale of the order of 20 ms, can

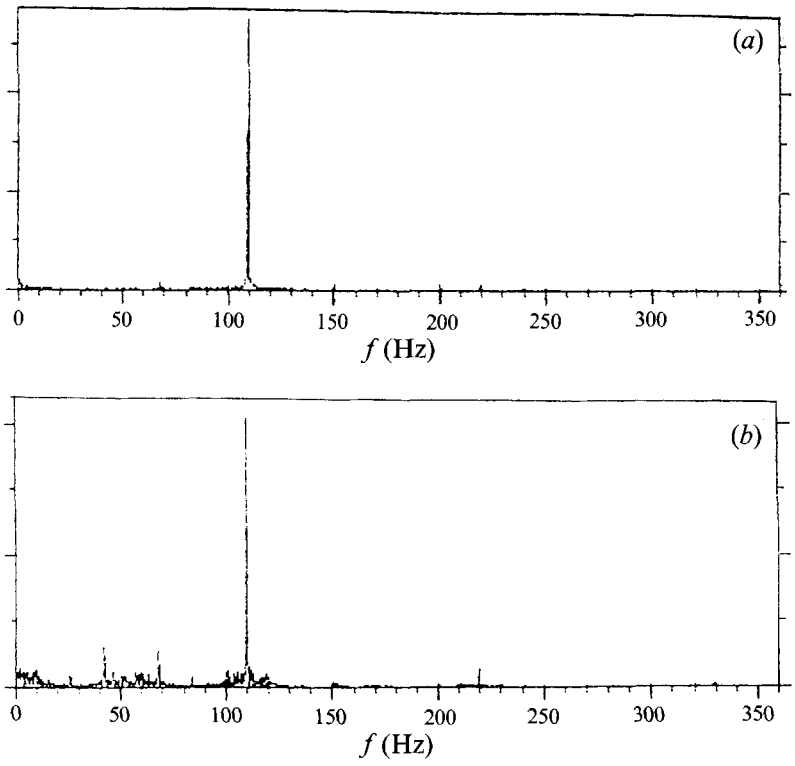

FIGURE 10. Spectrum without grid near branch II at forcing level (*a*) between G_1 and G_2, (*b*) G_2. $F = 100$, $U_0 = 10.2$ ms^{-1}.

be observed repeatedly (these are indicated with an arrow in figure 11). This may indicate that transitional structures develop in a deterministic way, although their appearance in time and space is random. Figure 11(*b*) shows oscilloscope traces for the moderate amplitude (G_2). The generated TS-wave is clearly visible, and its frequency (70 Hz) is readily seen in the graph. There are more transitional structures, but developed turbulent spots are still rare. When looking at the wave just in the vicinity of the transitional structures, a distinct frequency modulation is seen, resulting in approximately twice the wavelength of the fundamental TS-wave, which may be an indication of a subharmonic interaction. The last set of traces, shown in figure 11(*c*), are measured with the highest ribbon amplitude (G_3). They show strong intermittency and contain many turbulent spots.

In summary, the observations with and without the grid are quite different, and the wave forms observed in the presence of FST cannot readily be identified with either the K- or the N-regime of transition.

5.2. *Spanwise coherence of the wave fronts*

The general impression gained from the above observations is that the waves become significantly modified as they develop downstream. Although the ribbon initially sets up a two-dimensional wave front, randomly moving large-scale structures may lead to three-dimensional deformations of the wave fronts, which can cause local changes in both frequency and phase. Such waves are not captured by the phase-selective filtering technique used in §4, which only measures the part of the wave that is phase-locked to the ribbon.

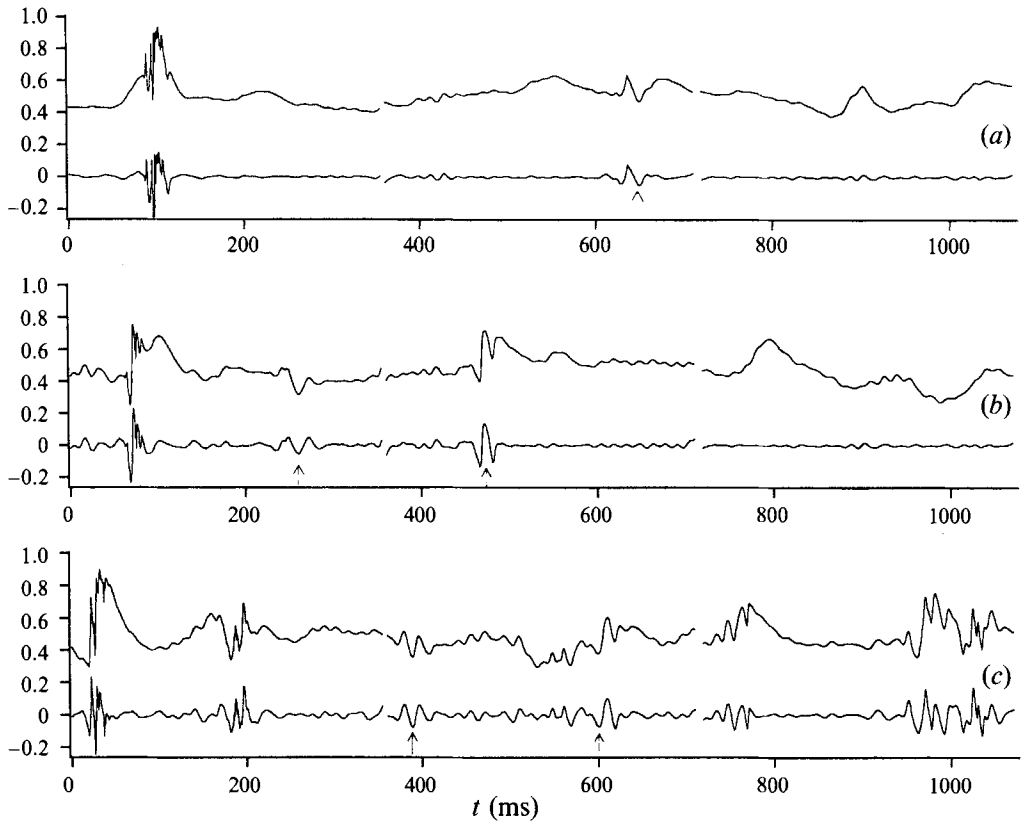

FIGURE 11. Selected hot wire traces (full signal and high-pass filtered above 30 Hz). Ribbon forced at $F = 100$ with amplitude (*a*) G_1, (*b*) G_2, (*c*) G_3. $x = 1000$ mm ($R = 1260$), y near TS-wave maximum.

One way of assessing to what extent the wave is two-dimensional, is to measure the correlation ($R_{uu,F}$) between two probes which are displaced in the spanwise direction, in the frequency band corresponding to the generator frequency. The phase-selective filtering method described in § 3 was not used in this measurement, so that the degree of phase-coherence with respect to the ribbon would not affect the measured correlation. If the shape of the wave front varies randomly, this will result in a varying phase difference between the probes, and thus a reduction of $R_{uu,F}$.

Figure 12 shows the value of $R_{uu,F}$ in a narrow band near $F = 100$, when the ribbon was forced with an amplitude slightly higher than G_1. The y-position was close to the inner maximum of the TS-wave, and the spanwise probe separation (Δz) spanned a distance of about half a TS-wavelength. In the grid-absent case, it can be seen that the correlation is equal to one, as expected when the oscillation is caused by a pure two-dimensional wave. The solid symbols show the same measurement in the presence of the grid, measured at two downstream positions. At $R = 890$, $R_{uu,F}$ shows a constant value of 0.8 for all Δz larger than 4 mm. Further downstream ($R = 1260$) this value has decreased to about 0.4. For reference, the spanwise correlation in the considered frequency band measured at $R = 890$ is displayed for the case without any forcing of the ribbon, but with the high level of FST. The correlation shows a rapid decay of $R_{uu,F}$ with a small anti-correlation at a separation of about 6 mm, which is in agreement with the results obtained in part 1 (cf. figure 14).

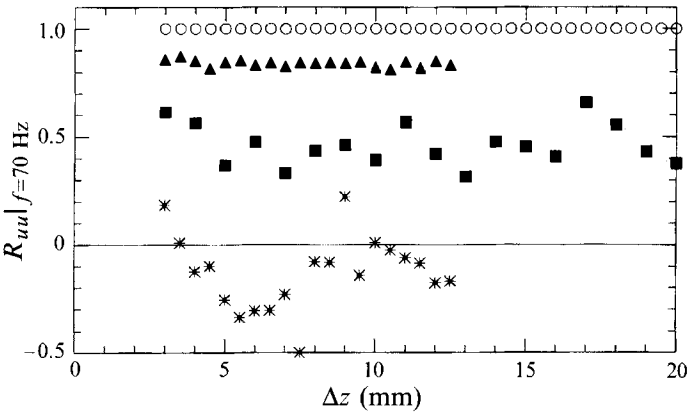

FIGURE 12. Spanwise correlations in a narrow band near the forcing frequency, $F = 100$; ○, without the grid, $R = 1260$; ▲, with the grid, $R = 890$; ■ with the grid, $R = 1260$; *, with the grid but without TS-wave forcing, $R = 890$.

The correlation is calculated as the cross-product of the two signals, normalized with both channels' r.m.s.-levels. A possible explanation for the lower correlation could be an increased contribution from disturbances with random phase, for instance if turbulent spots were not sorted out sufficiently. However, when comparing u_{rms}-levels in the considered frequency band the level has only increased by approximately 8% between the two x-positions. If the contribution from the two-dimensional part of the generated wave is assumed to be equal at both positions, this small increment in u_{rms} would reduce the spanwise correlation to 0.7, as compared with the measured value of 0.4. A second possible explanation of the small correlation could be a smaller TS-wave amplitude, but from the amplification curves shown in previous figures there is an increased amplitude between the two streamwise positions. Consequently, the downstream decay of $R_{uu,F}$ is mainly due to a distortion of the wave fronts of the generated TS-wave. If the three-dimensional distortion of the wave was caused by N- or K-type transition, the wave front should vary over a large spanwise scale, and the effects should be difficult to detect in figure 12. In the present measurements we also can observe a large reduction in the correlation curve at $R = 1260$ for very small spanwise separations ($\Delta z = 3$ mm). This rapid decay is in agreement with the curve obtained without any forcing of the ribbon, and thus substantiates the idea that the wave front distortion is associated with the large-amplitude disturbances with narrow spanwise scales that are induced by the FST.

5.3. *Nonlinearly induced TS-waves*

The above observations demonstrate that different kinds of interactions may be present, which would transfer energy between the waves, or between large-scale flow structures and waves. Some indications of the nature of such interactions may be obtained by analysing power spectra obtained at different forcing amplitudes.

The distributions presented in figure 13 represent energy spectra integrated in the near-wall region ($y/\delta^* < 1$), and normalized with the free stream velocity,

$$E = \frac{1}{\delta^* U_0^2} \int_0^{\delta^*} u_F'^2(y)\mathrm{d}y,$$

where $u_F'^2$ denotes the fluctuation energy within a 12 Hz square band close to the

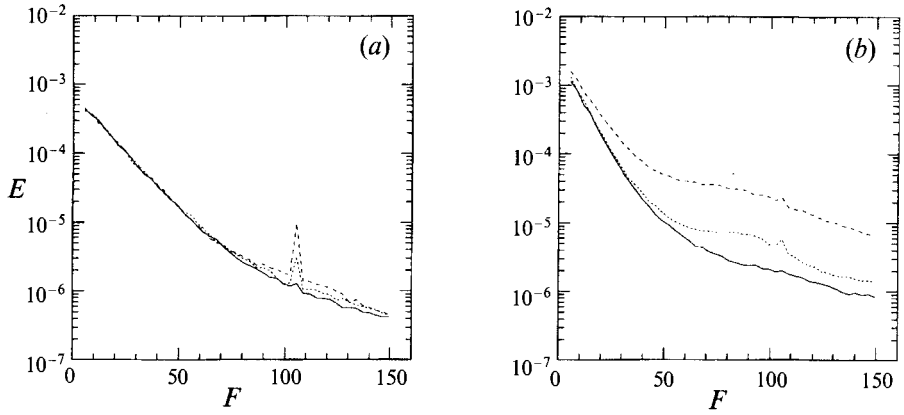

FIGURE 13. Energy integrated between $0 < y < \delta^*$ for different forcing amplitudes with $F = 100$. (*a*) $R = 890$, (*b*) $R = 1260$. —, G_1; ···, G_2; – – –, G_3.

frequency F. Each spectrum is the average of 50 sampling records, constructed without phase-alignment. Records containing turbulent spots were sorted out using the gradient criterion described in §3. The ribbon was forced at a frequency of $F = 100$, using different amplitudes (G_1, G_2 and G_3). The ribbon-generated wave gives a frequency peak which is clearly visible at $R = 890$ (figure 13*a*), but is difficult to distinguish at $R = 1260$ (figure 13*b*), because of an increase of the energy in a broad frequency band which includes the ribbon-generated wave. Upon increasing the ribbon amplitude, the energy growth is enhanced, and occurs within a wider frequency range. This dependence on the forcing amplitude shows that the induced wave packet is the result of nonlinear interactions, which involves the ribbon-controlled TS-wave.

The downstream increase in the induced energy can be observed even more clearly at a y-position close to the y-maximum in the TS-wave profile. In figure 14(*a–d*), each plot compares u'_F obtained at two x-positions, $x = 500$ mm and 1000 mm ($R = 890$ and 1260), for a given forcing amplitude. Figure 14(*a*) shows the spectrum when the generator is switched off. The downstream changes are rather small, and the perturbations actually decrease in the frequency band $30 < F < 70$. Figure 14(*b*) shows the spectrum when the ribbon is forced with an amplitude close to G_1. The energy is now seen to increase in a broad band between $F = 60$ and 120. This coincides with the frequency range where TS-waves are unstable (see figure 5); however, as G increases, the width of the induced energy band also increases. For the highest forcing amplitude (G_3, figure 14*d*), energy is already induced at the upstream position ($R = 890$). The new energy at $R = 890$ appears within the frequency range of unstable TS-waves; however, at $R = 1260$ it has increased at all frequencies. It is noteworthy that at both positions, the amplitude of the phase-coherent part of the G_3-wave, as measured with the phase-filtering technique, was only about 0.35% of U_0, and the amplification rate does not seem to be affected by nonlinearity (cf. figure 9*d*).

During the measurements, it was observed that the number of turbulent spots and transitional flow structures at $R = 1260$ increased drastically with ribbon amplitude. For the highest ribbon amplitude (G_3), 90% of the collected records were considered to be affected by intermittent turbulence. These records are not included in the data presented above. The observed energy growth is therefore not a mere reflection of an increase in the intermittency, but represents an increase of random fluctuations in the quiescent flow portions between the turbulent spots. However, the presence of

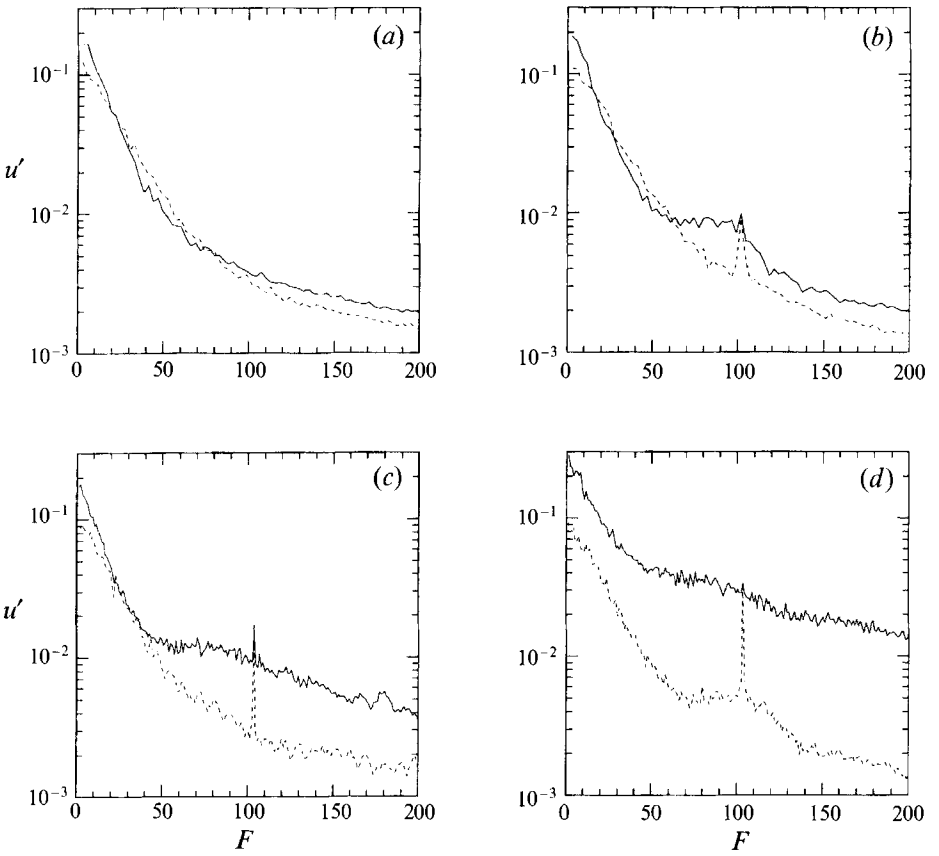

FIGURE 14. Comparison between upstream and downstream spectra at $y/\delta^* = 0.5$. Ribbon operating at $F = 100$, (*a*) no forcing, (*b*) G_1, (*c*) G_2, (*d*) G_3. ---, $R = 890$; —, $R = 1260$.

turbulent spots and bursts, even ones at a substantial distance from the sensor, may induce random motions in the layer by the action of the attendant pressure field. This may to some extent explain the broad-band increase in spectral energy, particularly for the case G_3 at $R = 1260$, for which the energy increases at all frequencies. Another explanation is that TS-waves are regenerated by nonlinear interactions between the forced wave and the background streak structures. The latter assumption is supported by the near-wall shape of the y-profiles of u'_F. Figure 15 compares profiles at $R = 890$ and 1260, filtered in 4 Hz bands centred at $F = 70$, 100 and 130, when the ribbon is operated at $F = 100$ with the amplitude G_2. All profiles have an outer maximum at $y/\delta^* = 2 - 2.5$, which is also present without forcing the ribbon. For $F = 100$, there is also a near-wall maximum at $y/\delta^* = 0.5$, which is due to the TS-wave excited by the ribbon. For $F = 70$ and 130, the profiles have a near-wall maximum only at the downstream position (filled symbols in figure 15), but not at the upstream position, which means that TS-waves are induced between the two positions. For frequencies $F > 150$ (not shown), the profiles of u'_F do not have any maximum at $y/\delta^* = 0.5$. For $F < 70$, contributions from other boundary layer perturbations are too large to allow an identification of a near-wall maximum. Unfortunately, this makes it difficult to detect the subharmonic of the original TS-wave.

From the data presented in figure 13, the downstream increase in the spectral energy for $70 < F < 130$ can be estimated to be a factor of 2 for the lowest ribbon

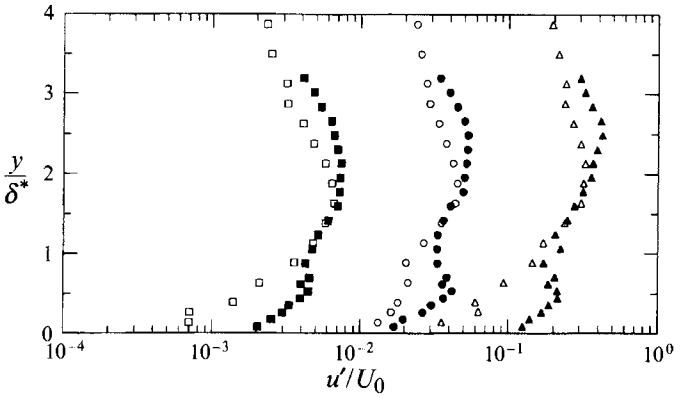

FIGURE 15. Comparison between upstream and downstream profiles of u'_F. □,■, $F = 70$; ○,●, $F = 100$; △,▲, $F = 130$. Open symbols, $R = 890$; filled symbols, $R = 1260$; Ribbon operating at $F = 100$ with amplitude G_2.

amplitude, and 10 for the highest amplitude, giving a value below 1.2 for an N-factor calculated as

$$N = \frac{1}{2} \ln \frac{E|_{R=1260}}{E|_{R=890}}.$$

Similar estimates based on the spectra at $y/\delta^* = 0.5$ give amplification factors between 2 ($N = 0.35$) and 25 ($N = 1.6$), for G_1 and G_3 respectively. Hence, the observed energy growth does not exceed the linear amplification of TS-waves in the absence of the grid ($N = 1.8$ for $F = 100$, cf. figure 9). Even for the highest ribbon amplitude (G_3), the amplitude of the coherent part of the wave (B) never exceeded 0.65% of U_0, and also the total value of u'_F was below 1%. It is therefore evident that in the presence of FST, TS-waves become 'dangerous' at much smaller amplitudes than in the undisturbed boundary layer.

6. Summary and discussion

The present observations can be summarized as follows.

(i) It is possible to generate and detect TS-like waves in a boundary layer subjected to FST with a level of at least 1.5%. The waves have mode shapes and phase velocities in close agreement with those of TS-waves in the absence of FST, and they move downstream as coherent wave trains. Their linear amplification rate is lower than in the undisturbed Blasius boundary layer.

(ii) During their downstream development, the wave fronts become increasingly three-dimensional, and lose part of their streamwise and spanwise coherence. At the same time, energy is induced within a frequency band which coincides with unstable TS-wave frequencies. This can already be observed at small amplitudes (B less than 0.2%). The downstream amplification of the induced energy increases with the forcing amplitude.

(iii) The presence of TS-waves leads to an increase in the number of turbulent spots, which promote the onset of transition. The process becomes explosive above a certain forcing amplitude ($\sim G_3$ in the present experiment).

The picture emerging from these observations lends itself to the following interpretation. Initially two-dimensional waves, riding on top of the large-scale streaky

structures, are gradually deformed due to diffraction-like interactions with the inhomogeneous background. This results in local changes in the phase and/or frequency of the wave. The distorted waves may continue to grow linearly, and as R increases, lower frequencies will amplify more rapidly. This scenario would favour subharmonic wave interactions, by which three-dimensional waves can be rapidly amplified. The process may be expected also to occur when TS-waves are induced naturally by the FST, since in this case the wave packets are three-dimensional from the beginning. If it occurs randomly in time and space, turbulence will not appear gradually along an ordered line, but in the form of localized turbulent spots.

It is necessary to make a distinction between the linear amplification rate of any single wave, and the energy growth resulting from nonlinearly induced waves. The phase-filtering technique used in § 4 only takes into account waves which maintain both their frequency and phase during their downstream development, and therefore only measures the linear amplification. The total energy growth in the TS-wave band is larger, and it depends on the amplitude of the input forcing. In all cases studied here, however, amplification rates were found to be below the growth rate of TS-waves in an undisturbed boundary layer. On the other hand, neither of these two growth measures is comparable to the growth rates obtained by Kosorygin & Polyakov (1990) or Kendall (1990, 1991) for naturally exited TS-waves, since in their case an increase of the TS-wave activity due to continuous downstream forcing is also included in the measured amplification rate.

The linear TS-wave amplification is smaller than that for TS-waves in a Blasius boundary layer, but larger than the amplification predicted by performing two-dimensional stability calculations for the measured mean velocity profile. This indicates that unsteady and/or three-dimensional effects have to be taken into account. If the large-scale perturbations are considered as randomly moving streak packets, the boundary layer may be considered locally as a spanwise-modulated flow. It could therefore be instructive to compare with experiments made in boundary layers with periodic spanwise non-uniformities. The development of TS-like waves in such flows has been studied e.g. by Kachanov & Tararykin (1987) and by Bakchinov *et al.* (1994), who found that the mode shapes, phase velocities and amplification rates depend not only on F and R but also on the intensity and spanwise scale of the modulation. This means that in a boundary layer subjected to FST, the TS-wave amplification rates may be expected to depend on the amplitude and typical spanwise scale of u_{rms} in the boundary layer, which in turn depend on the free stream characteristics.

The question of how the forced TS-waves induce energy at other frequencies might be a key question to solve in order to better understand transition in the presence of FST. The y-profiles in figure 15 indicate that the energy increase can be attributed to the generation of TS-waves at other frequencies than the forcing frequency. A noteworthy detail is that this occurs at rather low forcing amplitudes ($B < 0.2\%$ of U_0), where the amplification curve for the forced wave does not indicate any nonlinearity. The spectra in figure 14 are remarkably similar to those obtained by Gaster (1990) when controlled TS-waves were subjected to broad-band low-frequency noise. As in the present case, an increase in the TS-wave amplitude gave both a broadening of the frequency band and an increase in the amplification rate of the induced energy. The fact that energy is not generated at pure sub- or superharmonic frequencies may indicate that the interactions involve detuned subharmonics and their multiples, as observed in the experiment by Gaster. More exact information could be derived by analysing spectra from two-sensor measurements, and looking at the

bicoherence function as a means of identifying the onset of characteristic nonlinear motions (cf. Corke & Mangano 1989).

The present observations may also be compared to those made by Grek *et al.* (1991*a*) and Grek & Kozlov (1992), concerning interactions between TS-waves and so-called 'puffs'. Puffs are boundary layer structures excited by transient three-dimensional disturbances. They consist of narrow longitudinal streaks, which elongate in the downstream direction, and the perturbation has its maximum amplitude approximately in the middle of the boundary layer. These features are also observed in the boundary layer subjected to FST. In fact, the low-frequency boundary layer fluctuations observed in the presence of FST are most probably due to the passage of puff-structures, excited by turbulent eddies in the free stream. In the experiment of Grek *et al.*, different interactions were observed, depending on the amplitude of the TS-wave. When the TS-wave amplitude was small, the interaction generated a wave packet with a central frequency close to the subharmonic of the TS-wave, which further downstream developed into a turbulent spot. The present results are not sufficient to allow any further conclusions about transition mechanisms. However, model experiments of this type can give important clues to understanding the nonlinear processes preceding transition. Such experiments are presently being carried out within the Swedish–Russian research cooperation program.

This work was supported by the Swedish National Board for Industrial and Technical Development (NUTEK), and the Swedish Research Council for the Engineering Sciences (TFR). The visits of Professor V.V. Kozlov and Dr A.V. Boiko to Stockholm, as well as the visit of Dr B.G.B. Klingmann to Novosibirsk, were sponsored by the Royal Swedish Academy of Sciences (KVA) in cooperation with the Russian Academy of Sciences. We wish to thank Drs D. Arnal and J.C. Juillen, Dr J.M. Kendall, and the referees of this paper for valuable comments and discussion, and Ardeshir Hanifi for providing the codes for the stability calculations.

REFERENCES

ARNAL, D. & JUILLEN, J. C. 1978 Contribution expérimentale à l'etude de la receptivité d'une couche limite laminaire, à la turbulence de l'écoulement general. *ONERA Rapport Technique* No 1/5018 AYD, June 1978.

BAKCHINOV, A. A., GREK, G. R., KLINGMANN, B. G. B. & KOZLOV, V. V. 1994 Transition experiments in a spanwise-modulated boundary layer. *Phys. Fluids* (accepted).

BERTOLOTTI, F. P., HERBERT, T. & SPALART, P. R. 1992 Linear and nonlinear stability of the Blasius boundary layer. *J. Fluid Mech.* **242**, 441–474.

BLAIR, M. F. 1992 Boundary-layer transition in accelerating flows with intense freestream turbulence: Part 1 – Disturbances upstream of transition onset. *Trans. ASME* I: *J. Fluids Engng* **114**, 313–321.

BREUER, K. S. & HARITONIDIS, J. H. 1990 The evolution of a localized disturbance in a laminar boundary layer. Part 1. Weak disturbances. *J. Fluid Mech.* **220**, 569–594.

COHEN, J., BREUER, K. S. & HARITONIDIS, J. H. 1991 On the evolution of a wave packet in a laminar boundary layer. *J. Fluid Mech.* **225**, 575–606.

CORKE, T. C. & MANGANO, R. A. 1989 Resonant growth of three-dimensional modes in transitioning Blasius boundary layers. *J. Fluid Mech.* **209**, 93–150.

FASEL, H. 1990 Numerical simulation of instability and transition in boundary layer flows. In *Laminar-Turbulent Transition 3* (ed. D. Arnal & R. Michel), pp. 587–598. Springer.

GASTER, M. 1990 The nonlinear phase of wave growth leading to chaos and breakdown to turbulence in a boundary layer as an example of an open system. *Proc. R. Soc. Lond.* A **430**, 3–24.

GASTER, M. & GRANT, I. 1975 An experimental investigation of the formation and development of a wave packet in a laminar boundary layer. *Proc. R. Soc. Lond.* A **347**, 253–269.

GREK, H. R., DEY, J., KOZLOV, V. V., RAMAZANOV, M. P. & TUCHTO, O. N. 1991*a* Experimental analysis of the process of the formation of turbulence in the boundary layer at higher degree of turbulence of windstream. *Rep. 91-FM-2, Indian Inst. Science, Bangalore, 560012, India.*

GREK, H. R. & KOZLOV, V. V. 1992 Interactions between Tollmien-Schlichting waves and localized disturbances. *Siberian Phys.-Tech. J.* **5**, 68–76 (in Russian).

GREK, H. R., KOZLOV, V. V. & RAMAZANOV, M. P. 1985 Three types of disturbances from the point source in the boundary layer. In *Laminar-Turbulent Transition 2* (ed. V. V. Kozlov), pp. 267–272. Springer.

GREK, H. R., KOZLOV, V. V. & RAMAZANOV, M. P. 1987 Laminar-turbulent transition in the presence of a high level of free-stream turbulence. *Preprint No. 8-87*, USSR Academy of Sciences, Institute of Theor. and Appl. Mechanics, Novosibirsk (in Russian, English transl. 1988 in *Fluid Dyn.* **23**:6, 829–834).

GREK, H. R., KOZLOV, V. V. & RAMAZANOV, M. P. 1989 Investigation of boundary layer stability in the presence of a high degree of free-stream turbulence. In *Proc. of Intl Seminar on Problems of Wind Tunnel Modeling*, Vol I. Novosibirsk (in Russian).

GREK, H. R., KOZLOV, V. V. & RAMAZANOV, M. P. 1990*a* Investigation of boundary layer stability in a gradient flow with a high degree of free-stream turbulence. *Izv. Akad. Nauk SSSR, Mekh. Zhid. Gaza* **2**, 52–58 (in Russian, English transl. 1990 in *Fluid Dyn.* **25**:2, 152–156).

GREK, H. R., KOZLOV, V. V. & RAMAZANOV, M. P. 1990*b* Receptivity and stability of the boundary layer at a high turbulence level. In *Laminar-Turbulent Transition 3* (ed. D. Arnal & R. Michel), pp. 511–521. Springer.

GREK, H. R., KOZLOV, V. V. & RAMAZANOV, M. P. 1991*b* Laminar-turbulent transition at a high free stream turbulence level. *Siberian Phys.-Tech. J.* **6**, 106–138 (in Russian).

GULYAEV, A. N., KOZLOV, V. E., KUZNETSOV, V. R., MINEEV, B. I. & SEKUNDOV, A. N. 1989 Interaction of a laminar boundary layer with external turbulence. *Izv. Akad. Nauk SSSR, Mekh. Zhid. Gaza* **5**, 55–65 (in Russian, English transl. 1990 in *Fluid Dyn.* **24**:5, 700–710).

HENNINGSON, D. S., LUNDBLADH, A. & JOHANSSON, A. V. 1993 A mechanism for bypass transition from localized disturbances in wall-bounded shear flows. *J. Fluid Mech.* **250**, 169–207.

JORDINSON, R. 1970 The flat plate boundary layer. Part 1. Numerical integration of the Orr-Sommerfeld equation. *J. Fluid Mech.* **43**, 801–811.

KACHANOV, Y. S. 1987 On the resonant nature of the breakdown of a laminar boundary layer. *J. Fluid Mech.* **184**, 43–74.

KACHANOV, Y. S. 1994 Physical mechanisms of laminar-boundary-layer transition *Ann. Rev. Fluid Mech.* **26**, 411–482.

KACHANOV, Y. S. & LEVCHENKO, V. Y. 1984 The resonant interaction of disturbances at laminar-turbulent transition in a boundary layer. *J. Fluid Mech.* **138**, 209–247.

KACHANOV, Y. S. & TARARYKIN, O. I. 1987 Experimental investigations of an relaxating boundary layer. *Izv. SO Akad. Nauk SSSR, Tech. Nauk* **18**:5, 9–19 (in Russian).

KENDALL, J. M. 1985 Experimental study of disturbances produced in a pre-transitional laminar boundary layer by weak freestream turbulence. *AIAA Paper* 85-1695.

KENDALL, J. M. 1990 Boundary layer receptivity to freestream turbulence. *AIAA Paper* 90-1504.

KENDALL, J. M. 1991 Studies on laminar boundary layer receptivity to freestream turbulence near a leading edge. In *Boundary Layer Stability and Transition to Turbulence* (ed. D. C. Reda, H. L. Reed & R. Kobayashi), *ASME FED* **114**, 23–30.

KLEBANOFF, P. S., TIDSTROM, K. D. & SARGENT, L. M. 1962 The three-dimensional nature of boundary-layer instability. *J. Fluid Mech.* **12**, 1–34.

KLINGMANN, B. G. B. 1992 On transition due to three-dimensional disturbances in plane Poiseuille flow. *J. Fluid Mech.* **240**, 167–195.

KLINGMANN, B. G. B., BOIKO A. V., WESTIN, K. J. A., KOZLOV, V. V. & ALFREDSSON, P. H. 1993 Experiments on the stability of Tollmien-Schlichting waves. *Eur. J. Mech./B Fluids* **12**, 493–514.

KONZELMANN, U. 1990 Numerische Untersuchungen zur räumlichen Entwicklung dreidimensionaler Wellenpakete in einer Plattengrenzschichtsströmung. *PhD thesis*, Inst. A für Mechanik der Universität Stuttgart.

KOSORYGIN, V. S. & POLYAKOV, N. PH. 1990 Laminar boundary layers in turbulent flows. In *Laminar-Turbulent Transition 3* (ed. D. Arnal & R. Michel), pp. 573–578. Springer.

KOZLOV, V. E., KUZNETSOV, V. R., MINEEV, B. I. & SEKUNDOV, A. N. 1990 The influence of free-stream turbulence and surface ribbing on the characteristics of a transitional boundary layer. In *Near-Wall Turbulence. Proc. of 1988 Zorian Zaric Mem. Conf.* (ed. S. J. Kline & N. H. Afgan), pp. 172–189. Hemisphere.

MORKOVIN, M. V. 1984 Bypass transition to turbulence and research desiderata. In *Transition in Turbines. NASA Conf. Publ.* 2386, pp.161–204.

RAI, M. M. & MOIN, P. 1991 Direct simulation of transition and turbulence in a spatially evolving boundary layer. *AIAA Paper* 91-1607-CP.

SCHUBAUER, G. B. & SKRAMSTAD, H. K. 1948 Laminar boundary layer oscillations and transition on a flat plate. *NACA Rep.* 909.

SUDER, K. L., O'BRIEN, J. E. & RESHOTKO, E. 1988 Experimental study of bypass transition in a boundary layer. *NASA Tech. Mem.* 100913.

WESTIN, K. J. A., BOIKO, A. V., KLINGMANN, B. G. B., KOZLOV, V. V. & ALFREDSSON, P. H. 1994 Experiments in a boundary layer subjected to free stream turbulence. Part 1. Boundary layer structure and receptivity. *J. Fluid Mech.* **281**, 193–218.

ZELMAN, M. B. & MASLENNIKOVA, I. I. 1993 Tollmien-Schlichting-wave resonant mechanism for subharmonic-type transition. *J. Fluid Mech.* **252**, 449–478.